Pergamon

Int. J. Solids Structures Vol. 32, No. 16, pp. 2329–2344, 1995

0020-7683/95 $9.50 + .00

0020-7683(94)00252-5

ON THE BUCKLING/KINKING COMPRESSIVE FAILURE OF FIBROUS COMPOSITES†

I. CHUNG and Y. WEITSMAN‡
Department of Engineering Science and Mechanics, The University of Tennessee, Knoxville, TN 37996-2030, U.S.A.

(*Received* 25 *March* 1994; *in revised form* 21 *September* 1994)

Abstract—In this paper, it is demonstrated that the compressive response of unidirectionally reinforced composites may initiate in a micro-buckling mode and subsequently switch to a micro-kinked configuration. The foregoing possibility derives from a mechanics model that considers initial fiber misalignments, a non-linear shear response of the matrix, shear deformable fibers, and stochastic fiber spacings. The last-mentioned non-uniformity in fiber spacings plays a major role in the generation of fiber kinks.

Various features of the compressive deformation and failure process are exhibited by computational examples.

INTRODUCTION

The compressive response of composites has been studied extensively during the past three decades by many researchers. Many of the above studies are noted in comprehensive listings and review articles by Shuart (1985), Camponeschi (1991), Guynn *et al.* (1992), and Piggott (1993) and will not be detailed here. Suffice it to say that experimental data on compressive response exhibit substantial scatter, which is partly attributable to variability of the loading mechanisms and partly due to its sensitivity to random material flaws and misalignments. On the other hand, many analytical and computational models predicted compressive strengths in excess of experimental values. This shortcoming led to an ongoing effort to construct more complicated models, which incorporate additional material and structural parameters, to achieve closer correlation between predictions and data.

An intriguing aspect of the compressive response of fibrous composites is their failure by kinking. In most circumstances, post-failure inspections reveal the presence of tilted bands of broken fibers, separated along oblique straight lines from the remainder of the test sample. Since the formation of these so-called kink bands does not appear to accord with a buckling mode of failure, most existing models address the compressive failure of composites either as a buckling or as a kinking phenomenon, to the exclusion of the other. These models can be grouped as follows.

(1) Models that consider buckling

These include the work of Rosen (1965), which seems to be the first paper on compressive failure of composites. Considering "shear-mode buckling" that model predicted a failure stress $\sigma_{CR} = G_m/(1-\phi_f)$, where G_m is the shear modulus of the matrix and ϕ_f the fiber volume fraction. That prediction is inadequate for two reasons: (*a*) it gives a value of σ_{CR} that is several times as high as experimental values, (*b*) the relation $\sigma_{CR} \sim \{1/(1-\phi_f)\}$ contradicts experimental observations, which show that σ_{CR} grows linearly with ϕ_f (at least up to $\phi_f \approx 0.55$) [see Piggott and Harris (1980), Morley (1987)].

Several modifications to Rosen's model were introduced subsequently. Primarily, these modifications considered the non-linear shear response of the matrix and initial fiber waviness [e.g. Wang (1978), Lin and Zhang (1992), Guynn *et al.* (1992), Highsmith *et al.* (1992) and others listed in the aforementioned review articles]. Additional modifications included the incorporation of fibers' shear deformation, as by Davis (1975), or the accounting for large deformations of the fibers by Yin (1992). Though the latter model stems from

† Work supported under Contract N00014-90-J-1556 from the Office of Naval Research (ONR).
‡ Also at the Engineering Technology Division, Oak Ridge National Laboratory, U.S.A.

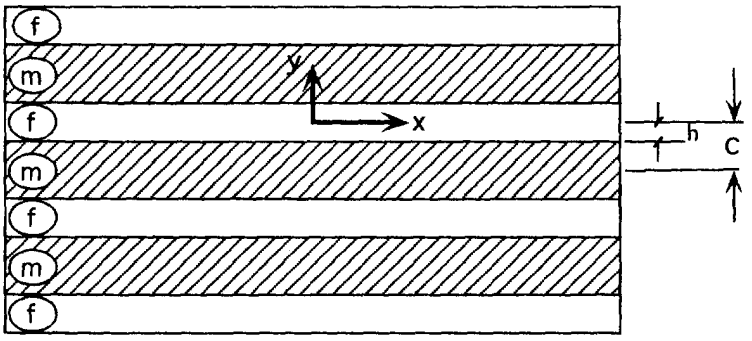

Fig. 1. The fiber-reinforced composite represented by a layered medium.

a buckling formulation, it is worth noting that it proposes a criterion for kink formation, which occurs when fibers' curvature attains a critical value.

(2) Models that consider the *a-priori* existence of kinks

These include work by Evans and Adler (1978), Hahn and Williams (1986), and Budiansky and Fleck (1992).

In all the above papers, the fiber-reinforced composites were viewed as lamellar regions that consist of fiber and matrix layers as shown in Fig. 1. It should be noted that several investigators [Sadowsky *et al.* (1967), Herrmann *et al.* (1967), Lanir and Fung (1972), and Greszczuk (1975)] considered fibers of cylindrical geometry. All these papers assumed linear elastic behavior of fiber and matrix materials.

The validity of representing fiber-reinforced materials as lamellar regions was questioned recently by Weitsman and Chung (1994), where severe disparities were shown to exist between the strain fields within a composite reinforced by hexagonal fibrous arrays undergoing buckling and analogous fields in a composite that consists of lamellar regions. This issue is the subject of an ongoing investigation.

The main purpose of the present paper is to present a model for the compressive response of fiber-reinforced composites that suggests a transitional mechanism from a micro-buckling form of deformation to a micro-kinking mode of failure. The model employs the lamellar geometry of Fig. 1 and incorporates a non-linear shear response of the matrix and linearly elastic, shear-deformable fibers. In addition, the model considers two kinds of geometrical imperfection, initial fiber wobbliness and non-uniform fiber spacing. The latter consideration is the novel aspect of this work. In closely spaced fibrous domains, the narrow matrix regions sustain increased levels of shear strains, which approach yield or failure limits. The resulting softening in the support provided by the matrix to the fibers is shown to cause localized fiber failures, accompanied by overburdening the more widely spaced fibers. Though compressive failure still occurs by buckling, the immediate post-buckled configuration is shown to consist of kinked fibers. The sudden transition from buckling to kinking is due to the abrupt variation in the deformed configuration that follows the buckling instability. This comprehensive accounting for the seemingly disparate phenomena of buckling and kinking is the main asset of the present model.

Non-uniform fiber spacings were considered by Chung and Weitsman in previous work (1994a). However, in that work, the response of the fibers was modelled by means of Bernoulli–Euler beam theory, which ruled out the formation of kinks, since that theory does not allow for shear deformations. It is interesting to note that, under the constraints inherent in the Bernoulli–Euler beam theory, the absence of kinks was compensated by the presence of highly concentrated shear forces in the post-buckling range of response. An abbreviated version of the current paper with computational results based upon material data reported by Guynn *et al.* (1992) appeared recently (Chung and Weitsman, 1994b).

BASIC EQUATIONS

Let a unidirectionally reinforced fibrous composite be represented by a layered medium that consists of fiber and matrix layers of thicknesses $2h$ and $2(c-h)$, respectively, as shown

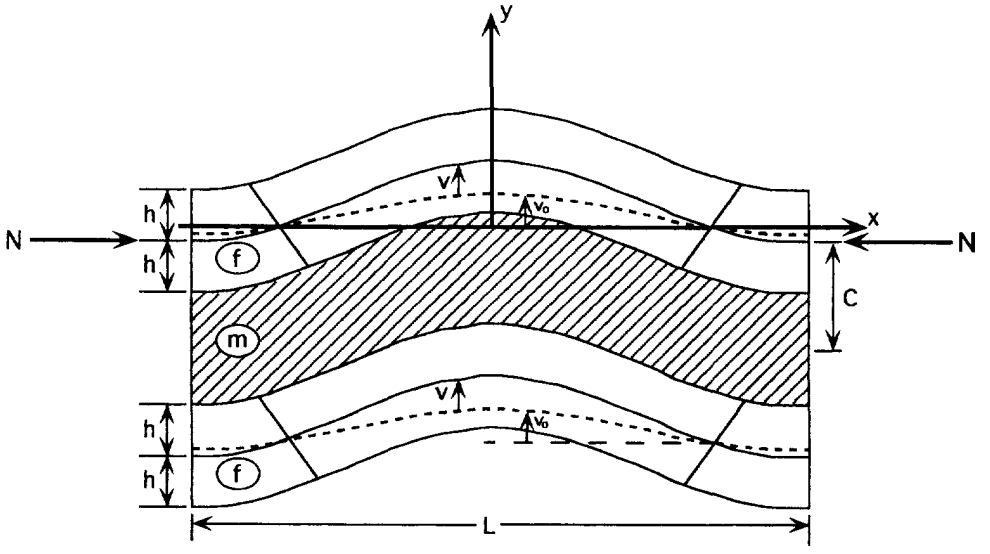

Fig. 2. The shear-mode buckling configuration.

in Fig. 1. Let $\phi_f = h/c$ and $\phi_m = (c-h)/c$ denote volume fractions where here, and in the remainder of this paper, subscripts f and m refer to the fiber and matrix, respectively. Let x and y denote co-ordinates parallel and normal to the layers, with corresponding displacements u and v.

Consider an initial waviness v_0 in the fiber layer, given by

$$v_0 = \delta_0 \cos(\pi x/L) \tag{1}$$

and let the fibers deflect in a shear mode of buckling as shown in Fig. 2 [Rosen (1965), Garg *et al.* (1973)].

The length L prescribes the micro-buckling length associated with compressive loading N parallel to the fibers. We assume that the matrix layer responds in shear only, sharing a common displacement v with the fiber, while u_m varies linearly in y across the layer's thickness. In addition, we assume that the response of the fiber layer can be modelled by Timoshenko's shear-deformation theory, where ψ denotes the independent rotation of the planar cross-section.

Accounting for bending effects, the total displacement of a fiber region U_f is given by [Washizu (1975)]

$$U_f = u_f + \tfrac{1}{2}\int_0^x [(v'+v_0')^2 - (v_0')^2]\,dx - y\psi \tag{2}$$

with the corresponding strains

$$\varepsilon_x^f = u_f' + \tfrac{1}{2}[(v'+v_0')^2 - (v_0')^2] - y\psi' \tag{3a}$$

$$\gamma_{xy}^f = v' - \psi \tag{3b}$$

while

$$\gamma_{xy}^{m} = \frac{\partial v}{\partial x} + \frac{\partial u_m}{\partial y} = v' + \frac{1}{2(c-h)}[U_f(x, 2c-h) - U_f(x, h)]$$

$$= v' - \frac{\phi_f}{\phi_m}\frac{\partial U_f}{\partial y} = v' + \frac{\phi_f}{\phi_m}\psi. \tag{4}$$

In eqns (2)–(4), and in the sequel, primes denote derivatives with respect to x.

Consider a linear elastic response for the fibers

$$\sigma_x^f = E_f \varepsilon_x^f, \quad \tau_{xy}^f = G_f \gamma_{xy}^f \tag{5}$$

and a non-linear shear stress–strain response for the matrix, scaled by the initial shear modulus G_m^e

$$\tau_{xy}^m = G_m^e \, F(\gamma_{xy}^m). \tag{6}$$

The total relative deflection between $x = 0$ and $x = L/2$ is given by

$$\Delta = u_f(L/2) + \tfrac{1}{2}\int_0^{L/2} [(v' + v_0')^2 - (v_0')^2] \, dx. \tag{7}$$

RANDOM FIBER SPACING

As noted in the Introduction, random fiber spacing accounts for an essentially novel feature in the present model. Recalling basic notions concerning the statistics of spatially distributed data and the concept of Voronoi cell tessellation, as employed to represent the spatial distribution of spherical and cylindrical inclusions within an extended matrix region (Davy and Guild, 1988), we assume that the cell sizes $2c$ are distributed according to a Poisson's point process, with a cumulative distribution function

$$P(C > c) = \exp(-c/\bar{c}). \tag{8}$$

In eqn (8), $2\bar{c}$ is the nominal average of the cell sizes. Since fiber regions cannot overlap, namely $c > h$ ("Gibb's hard core process"), eqn (8) is modified to read

$$P(C > c) = \exp\left(-\frac{c-h}{\bar{c}-h}\right). \tag{9}$$

The corresponding probability distribution is

$$p(c) = -\frac{1}{\bar{c}-h}\exp\left(-\frac{c-h}{\bar{c}-h}\right). \tag{10}$$

Since eqn (4) expresses γ_{xy}^m in terms of ϕ_f and $\phi_m = 1 - \phi_f$, rather than c, it is necessary to recast $p(c)$ in terms of a probability distribution of the fiber volume fractions $p(\phi_f)$, where $\phi_f = h/\bar{c}$. Employing well-established rules of statistical analysis, we obtain

$$p(\phi_f) = \frac{\bar{\phi}_f}{\bar{\phi}_m}\frac{1}{\phi_f^2}\exp\left(-\frac{\bar{\phi}_f}{\bar{\phi}_m}\frac{\phi_m}{\phi_f}\right). \tag{11}$$

For computational purposes, the distribution function $p(\phi_f)$ will be discretized and expressed by a finite number of Dirac delta functions.

FIELD EQUATIONS FOR RANDOMLY SPACED LAYERS IN COMPRESSION

From eqn (4), and subsequently eqn (6), it follows that both γ_{xy}^{m} and τ_{xy}^{m} are functions of the random variable ϕ_f and thereby random as well. However, to ascertain a common displacement Δ for all layers, we assume identical displacements u and v for all layers in spite of the randomness in their widths $2c$. We surmise that the effects of random spacing are taken up by distinct values of the rotation ψ, which vary from layer to layer. Consequently, a discretized version of $p(\phi_f)$ that corresponds to M values of $(\phi_f)_i$ $(i = 1, \ldots M)$ will necessitate the consideration of M values of $\psi_i (i = 1, \ldots M)$.

The above assumption involves an approximation whose validity can be estimated. It will be shown below that a solution for u, v, $\psi_1, \ldots \psi_M$ that is based upon energy considerations for the entire composite fails to satisfy equilibrium conditions for any of the M individual layers. The magnitudes of the unequilibrated transverse forces (distributed transverse loads $q_i(x)$, $i = 1, \ldots M$) provide the required estimate of error. It turns out that the above magnitudes never exceed 1% of all calculated stress values, attesting to the suitability of the approximation.

Application of the principle of virtual work to the entire composite [Washizu (1975)], upon accounting for the randomness of the cell sizes c, yields

$$\int_h^\infty p(c)\left\{\int_{V_f}(\sigma_x^f\delta\varepsilon_x^f+\tau_{xy}^f\delta\gamma_{xy}^f)\,\mathrm{d}V_f+\int_{V_m}\tau_{xy}^m\delta\gamma_{xy}^m\,\mathrm{d}V_m\right\}_{(c)}\mathrm{d}c+N\delta\Delta=0. \tag{12}$$

From eqns (3)–(6), which contain the random variables ϕ_f and ϕ_m, and since by hypothesis ψ depends on c, it follows that the expression inside the parenthesis on the left side of eqn (12), which applies for a cell of size c, is a function of the random variable c.

Consider a discrete probability distribution, represented by W_i, commensurate with eqns (10) and (11), which corresponds to M cells of widths $2c_i$ $(i = 1, \ldots M)$. In this case, the integral in eqn (12) is replaced by a sum, and we obtain

$$2\sum_{i=1}^{M}W_i\int_0^{L/2}\left\{\int_0^{h}(\sigma_x^f\delta\varepsilon_x^f+\tau_{xy}^f\delta\gamma_{xy}^f)\,\mathrm{d}y+\int_h^{c_i}\tau_{xy}^m\delta\gamma_{xy}^m\,\mathrm{d}y\right\}\mathrm{d}x+N\delta\Delta=0. \tag{13}$$

Note that $\delta\varepsilon_x^f$, $\delta\gamma_{xy}^f$ and $\delta\gamma_{xy}^m$ contain $M+2$ independent variables, namely δu, $\delta v'$ and $\delta\psi_i (i = 1, \ldots M)$.

Substitution of eqns (2)–(7) into eqn (13), integrating by parts, and collecting terms that multiply δu, $\delta v'$, and $\delta\psi_i (i = 1, \ldots M)$, we obtain the following $(M+1)$ field equations for v and $\psi_i (i = 1, \ldots M)$

$$-N(v'+v_0')+2h\sum_{i=1}^{M}\{G_f(v'-\psi_i)+(\phi_m/\phi_f)_iG_m^e\mathrm{F}[v'+(\phi_f/\phi_m)_i\psi_i]\}=0 \tag{14}$$

$$-E_fI_f\psi_i''-2hG_f(v'-\psi_i)+2hG_m^e\mathrm{F}[v'+(\phi_f/\phi_m)_i\psi_i]=0 \quad (i=1,\ldots M) \tag{15}$$

with the boundary conditions

$$\psi_i'(L/2)=0, \quad \psi_i(0)=0 \quad (i=1,\ldots M), \quad \text{and} \quad v'(0)=0. \tag{16}$$

Note that the coupled system of eqns (14) and (15) is non-linear because of the presence of the function F, which is non-linear in its argument.

In eqn (15), $I_f = h^3/12$. Note that the variation δu yields the trivial result N = constant = N_{applied} and requires no further consideration.

Unlike eqns (15), which apply to the M individual cells, eqn (14) expresses the lateral equilibrium of the entire composite. To ascertain the lateral equilibrium of each cell it is necessary to impose distributed transverse loads $q_i(x)$ $(i = 1, \ldots M)$ and consider their virtual work

$$\int_0^{L/2} q_i \delta v \, \mathrm{d}x.$$

Re-employing the principle of virtual work for each individual cell, collecting terms that multiply δv, and utilizing the solution for v and ψ_i, which corresponds to the system of eqns (14)–(16), we obtain

$$q_i = N(v'' + v_0'') - 2h\{G_f(v'' - \psi_i') + (\phi_m/\phi_f)_i G_m^e \mathrm{F}'[v' + (\phi_f/\phi_m)_i \psi_i]\}. \tag{17}$$

The relative magnitudes of q_i/τ_{xy}^m serve as measures for the validity of the approximation inherent in assuming common u and v in all layers. It will be shown in the next section that, for polymeric composites, all the above ratios appear to be less than 10^{-2}.

A non-dimensional version of eqns (14) and (15) is obtained upon introducing $X = x/L$, $V = v/L$, and the non-dimensional factors

$$\alpha_f^2 = \frac{2G_f h L^2}{E_f I_f}, \quad \alpha_m^2 = \frac{2G_m^e h L^2}{E_f I_f}, \quad \lambda^2 = \frac{NL^2}{E_f I_f}.$$

Then, upon putting $Y = \mathrm{d}V/\mathrm{d}X$, eqns (14) and (15) read

$$-\lambda^2(Y + Y_0) + \alpha_f^2 Y + \sum_{i=1}^{M} W_i\{-\alpha_f^2 \psi_i + (\phi_m/\phi_f)_i \alpha_m^2 \mathrm{F}[Y + (\phi_f/\phi_m)]_i \psi_i\} = 0 \tag{18}$$

and

$$\psi_i'' + \alpha_f^2(Y - \psi_i) - \alpha_m^2 \mathrm{F}[Y + (\phi_f/\phi_m)_i \psi_i] = 0 \quad (i = 1, \ldots M) \tag{19}$$

with the boundary conditions

$$\psi_i'(1/2) = 0, \quad \psi_i(0) = 0, \quad (i = 1, \ldots M) \quad \text{and} \quad Y(0) = 0. \tag{20}$$

RESULTS

The solution to eqns (18)–(20) was obtained numerically and pertains to graphite/PEEK (APC-2) composites. The interval $0 < X < 1/2$ was subdivided into K equal subintervals, and derivatives were expressed by means of central finite differences. The discretized system of equations was solved iteratively to obtain values of V and ψ_i for increasing load N in the pre-buckling range. In accordance with observations by Johnson *et al.* (1991), the matrix material was assumed to fail in those regions where $\gamma_{xy}^m \geqslant 0.05$. The response in the post-buckling range was evaluated by prescribing the location X^* where $\gamma_{xy}^m = 0.05$ in the most recently failed cells and evaluating the corresponding deflected shape $V(X)$ and applied load N.

Complete details are given in the Appendix.

The computations employed values of $E_f = 214$ GPa and $G_f = 13.8$ GPa, which reflect the significant transverse isotropy of the AS4 fibers [Aboudi (1991)]. The *in-situ* shear stress–strain response of the PEEK resin was based upon the reduction of data collected

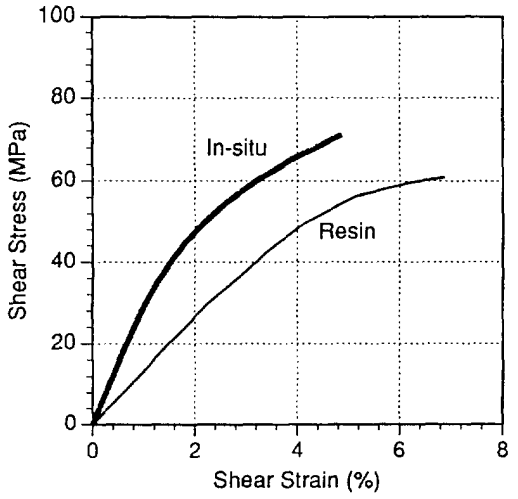

Fig. 3. Non-linear shear response of PEEK at 21°C. *In-situ* response is reduced from composite AS4/PEEK data by Kyriakides and Liechti (1993) and compared with the behavior of neat resin.

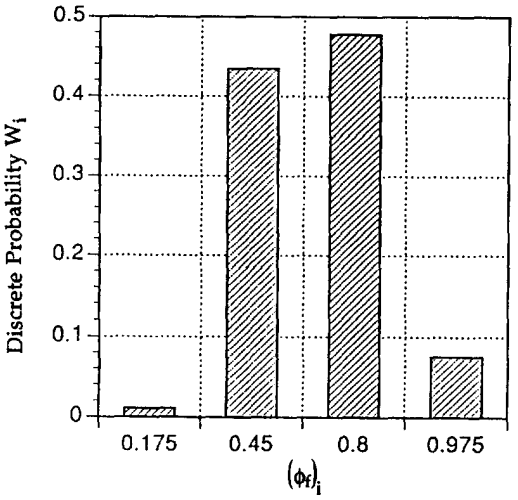

Fig. 4. The selected discretization of the random distribution expressed in eqn (10) into four distinct values of ϕ_f, with average value $\bar{\phi}_f = 0.6$.

by Kyriakides and Liechti (1993). The *in-situ* data are shown in Fig. 3, where they are contrasted with data for unreinforced PEEK.

The *in-situ* shear data were expressed by the relation

$$\gamma = \frac{\tau}{A} + \left(\frac{\tau}{B}\right)^{1/q}$$

where $A = 3096$ MPa, $B = 169.93$ MPa, $q = 0.23781$, and τ is in MPa. As noted earlier, shear failure was assumed to occur at a strain of $\gamma_u = 0.05$. In addition, we took $L = 400d$ and $\delta_0 = 4d$, as suggested by Kyriakides and Liechti (1993), with a fiber diameter $d = 7.6$ μm.

The computational scheme considered four random cell sizes, namely four discrete random values of ϕ_f that accord with the distribution function of eqn (11). These are shown in Fig. 4.

Computational results are shown in Figs 5–12.

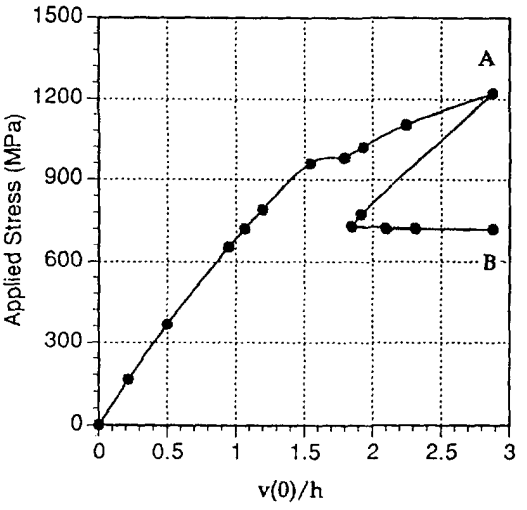

Fig. 5. Applied stress vs non-dimensional maximal lateral deflection $v(0)/h$. The pre-buckling stage 0A is followed by the post-buckling stage AB.

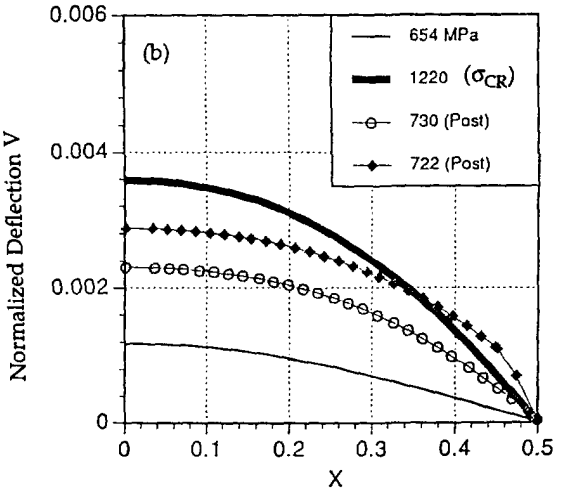

Fig. 6. Plots of the non-dimensional deflection V vs the non-dimensional distance X at various levels of applied stress.

Figure 5 exhibits the variation of the applied stress σ with the non-dimensionalized maximal lateral deflection $v(0)/h$. The short plateau-like region at $1.5 < v(0)/h < 1.8$ is due to matrix failure, which initiates and spreads within the cell with the highest fiber volume fraction ($\phi_f = 0.975$). Failure by buckling occurs at $\sigma = 1220$ MPa (point A). In a displacement-controlled experiment, a further increase in Δ will be accompanied by a drop in σ and a corresponding reduction in $v(0)/h$. The post-buckling response is represented by the segment AB in Fig. 5.

Results for the non-dimensionalized displacement V and slope Y are plotted versus the non-dimensional distance X in Figs 6 and 7 for various load levels in both pre- and post-buckling ranges. As may be expected, these curves are approximately proportional to cos X and sin X in the pre-buckling range, where deformed shapes are dominated by the form of the initial misalignment. Note, however, the substantial deviations in the deformed configurations within the post-buckling range, where they no longer resemble the cos X shape of the initial misalignment. The most significant departures occur near $X = 0.5$, where matrix failures initiate.

The distributions of τ^m_{xy} versus X are plotted in Figs 8(a)–8(d). These distributions are shown within the four distinct cells and for various levels of applied stress. Figure 8(a) corresponds to a pre-buckled stress level $\sigma = 654$ MPa, and Fig. 8(b) corresponds to the

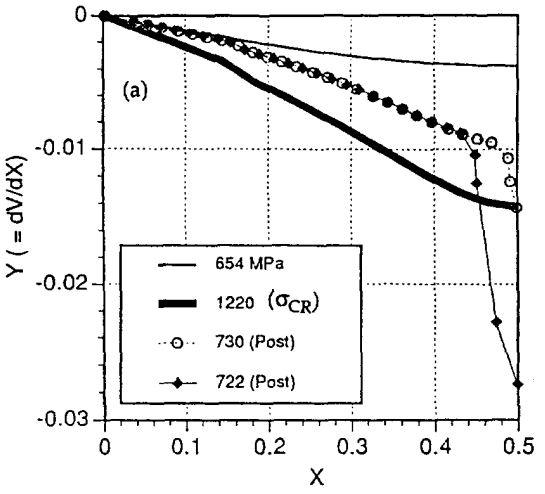

Fig. 7. Plots of the non-dimensional slope Y vs the non-dimensional distance X at various levels of applied stress.

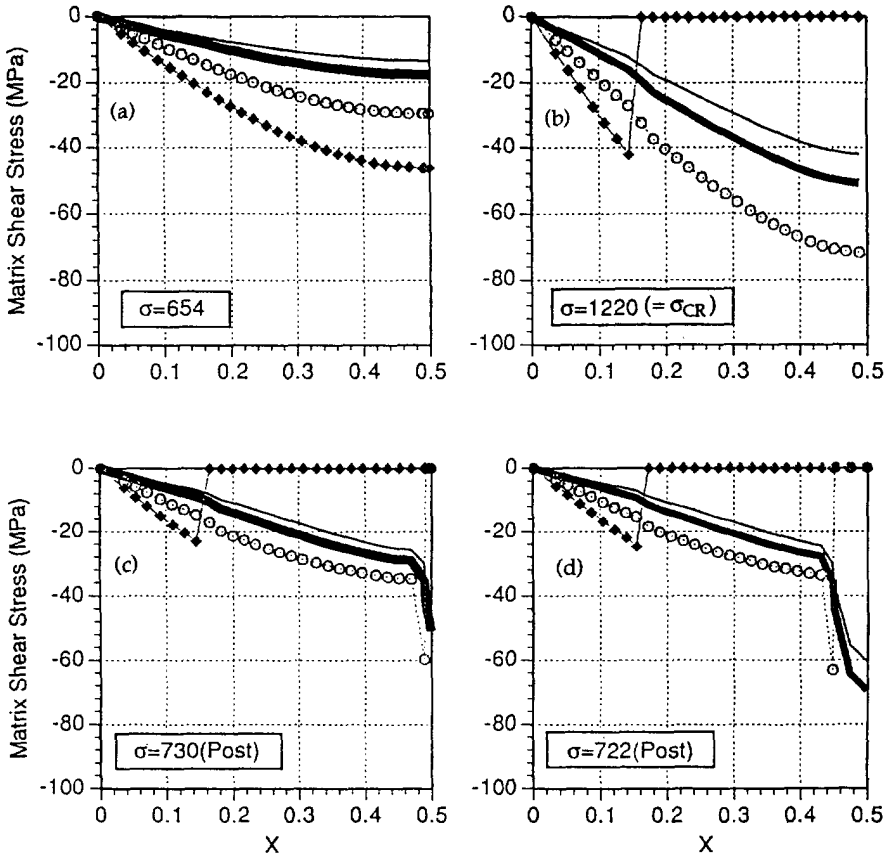

Fig. 8. The distribution of matrix shear stress vs the non-dimensional distance X within the four distinct cells (—— $\phi_f = 0.175$; —— $\phi_f = 0.45$; ○○○○○ $\phi_f = 0.8$; ◆◆◆◆◆ $\phi_f = 0.975$) at various levels of applied stress: (a) $\sigma = 654$ MPa (pre-buckling); (b) $\sigma = 1220$ MPa (buckling); (c) $\sigma = 730$ MPa (post-buckling); and (d) $\sigma = 722$ MPa (post-buckling. Point B in Fig. 5).

buckling stress $\sigma = 1220$ MPa (point A in Fig. 5) when the matrix within the cell with $\phi_f = 0.975$ failed over the range $0.16 < X < 0.5$.

Figures 8(c) and 8(d) correspond to post-buckling loads of $\sigma = 730$ MPa and $\sigma = 722$ MPa, respectively. The latter stress corresponds to point B in Fig. 5, which lies directly below point A in that figure. Note the spreading of the failure region in the cell with $\phi_f = 0.8$

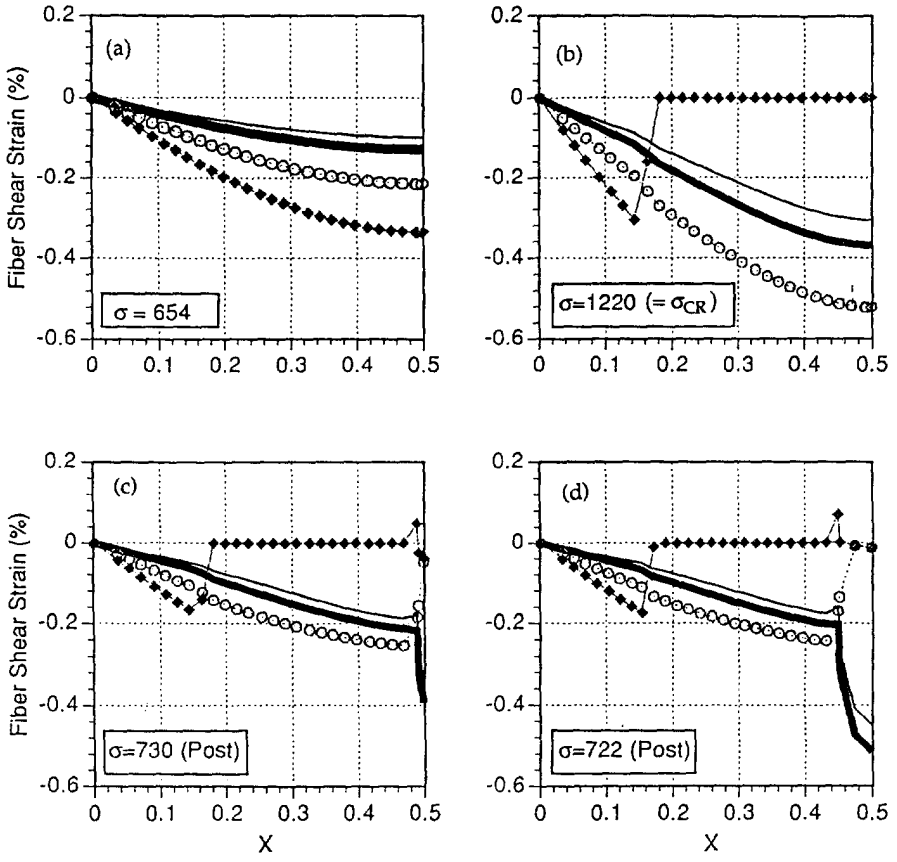

Fig. 9. The distribution of fiber shear strain vs the non-dimensional distance X in the four distinct cells (symbols and stress levels the same as in Fig. 8).

between the post-buckling stages depicted in Figs 8(c) and 8(d). This means that matrix failure, which was confined to $0.49 < X < 0.5$ at $\sigma = 730$ MPa expanded over $0.45 < X < 0.5$ as the post-buckling load level proceeded to drop to $\sigma = 722$ MPa. There were also increases in τ^{m}_{xy} within the unfailed cells with $\phi_f = 0.45$ and $\phi_f = 0.175$.

The central theme of the present article is demonstrated in Figs 9(a)–9(d). These figures exhibit the fiber shear strains γ^{f}_{xy} versus the non-dimensional distance X for the same circumstances as in Figs 8(a)–8(d). The essential feature of these figures develops within the post-buckling range, where *discontinuities* in γ^{f}_{xy} are noted to occur simultaneously within all cells. These discontinuities are located at $X = 0.49$ in Fig. 9(c) and at $X = 0.45$ in Fig. 9(d). No such discontinuities exist in the pre-buckling stage or at buckling.

We suggest that the foregoing discontinuities in γ^{f}_{xy} portend the onset of fiber kinking.

Figure 10(a) exhibits the computed values of the lateral loads $q_i(X)$ versus X within all four cells at buckling, namely at $\sigma = 1220$ MPa. These loads, which were evaluated through eqn (17), are much smaller than $\tau_u = 70$ MPa, attesting to the validity of the premises of the present model. For purposes of comparison, the same lateral loads are plotted versus X in Fig. 10(b) when the fibers are modelled as Bernoulli–Euler beams by employing a previous analysis by Chung and Weitsman (1994a).

Additional effects of random fiber spacings are exhibited in Figs 11 and 12. Figures 11(a) and 11(b) concern the evolution of fiber curvatures with load within the pre-buckling range and demonstrate the contrast between uniformly spaced and randomly spaced circumstances. It may be noted that the randomly spaced case and the onset of localized failures gives rise to highly concentrated curvatures, with magnitudes that exceed by three or four folds the levels that correspond to the uniformly spaced case. If one accepts the premise of Yin (1992) that kinks occur when a fiber's curvature exceeds a certain threshold

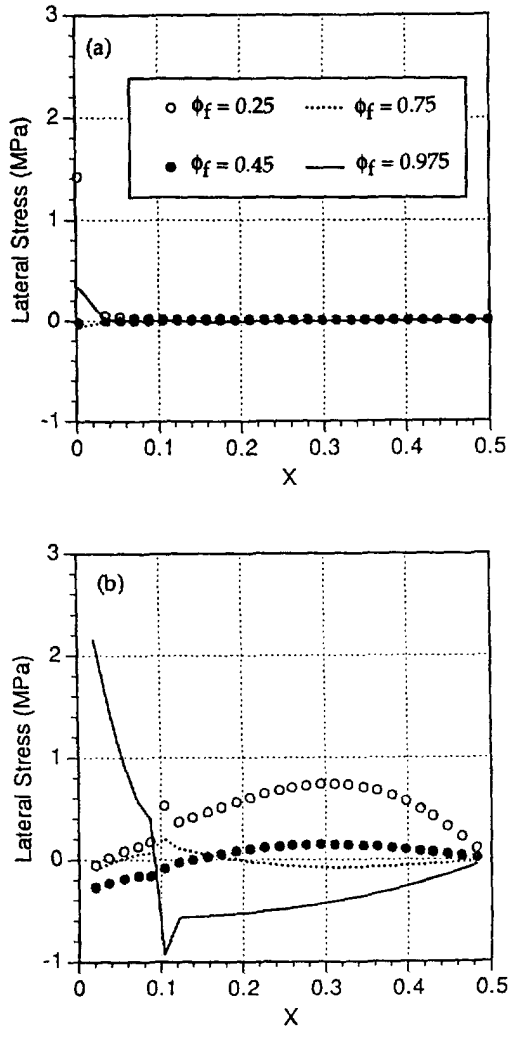

Fig. 10. Lateral stresses $q_i(x)$ at $\sigma = \sigma_{CR} = 1220$ MPa vs the non-dimensional distance X in the four distinct cells: (a) shear deformable fibers; (b) fibers deforming as Bernoulli–Euler beams. (○ $\phi_f = 0.25$; ● $\phi_f = 0.45$; ··· $\phi_f = 0.75$; —— $\phi_f = 0.975$).

level, then the current analysis indicates the existence of an enhanced likelihood of kinking due to non-uniform fiber spacing. Such kinking may precede failure by buckling.

Finally, the effect of random fiber spacing on compressive strength is shown in Fig. 12, where buckling failure loads are plotted versus the fiber volume fraction ϕ_f. The results for the random case were computed for average values $\bar{\phi}_f$ (with the distribution shown in Fig. 4) that are identical with the constant ϕ_f for the uniformly spaced case. Note that random fiber spacings result in lower strengths with $\bar{\phi}_f$, which accords with experimental observations by Piggott and Harris (1980).

CONCLUSIONS

A mechanics model was presented for the compressive response and failure of unidirectionally reinforced polymeric composites loaded parallel to the fiber direction. The analysis accounted for the non-linear shear response of the resin, including its ultimate shear strain, and for shear deformable fibers. The model incorporated two kinds of geometric imperfections, namely, initial fiber waviness and random fiber spacings. With the exception of the work by Chung and Weitsman (1994a,b), the latter kind of imperfection has not been considered elsewhere.

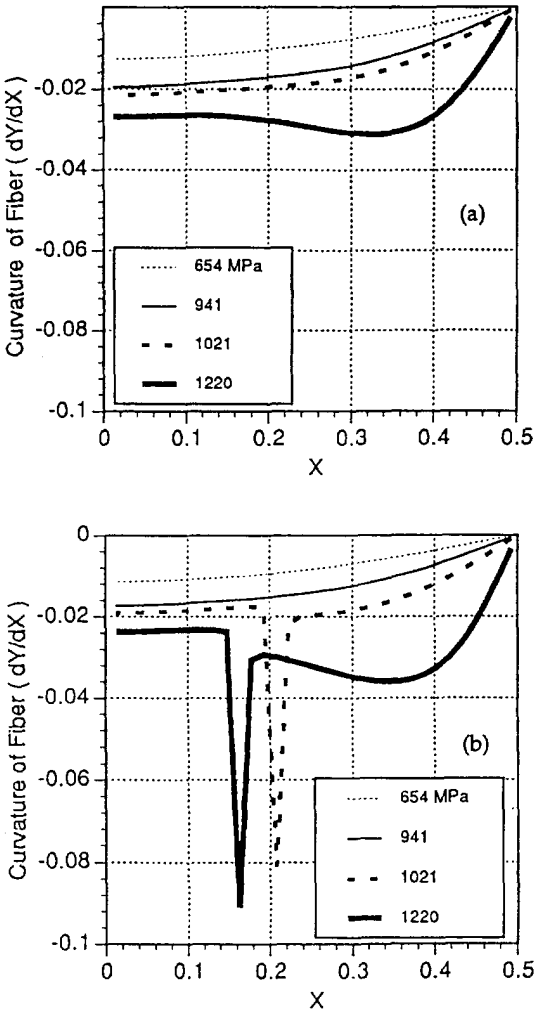

Fig. 11. Non-dimensional fiber curvatures (dY/dX) vs non-dimensional distance X at four levels of applied stress in the pre-buckling range (····· $\sigma = 654$ MPa; —— $\sigma = 941$ MPa; – – – $\sigma = 1021$ MPa; —— $\sigma = 1220$ MPa (buckling)): (a) uniformly spaced fibers with $\phi_f = 0.6$; (b) randomly spaced fibers (according to Fig. 4) with $\phi_f = 0.6$.

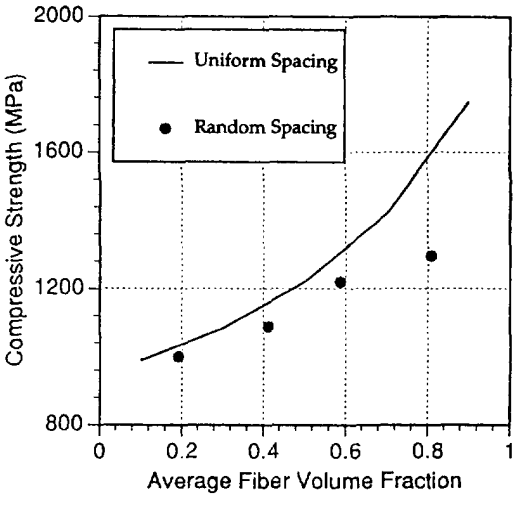

Fig. 12. Variation of compressive strength (= buckling load) with fiber volume fraction ϕ_f (= $\bar{\phi}_f$ in randomly spaced case). Comparison between uniformly and randomly spaced cases.

Computational results were evaluated within both pre- and post-buckling ranges of compressive response. The paramount result of this work is an indication that a band of discontinuity in the fibers' shear strains can occur immediately beyond failure by buckling. Such a discontinuity prognosticates the formation of kink bands, which are observed in many failed specimens.

It was shown that accounting for random fiber spacings results in lower predicted values of compressive strength which correlate better with data. In addition, the foregoing randomness yields a relationship between compressive strength and fiber volume fraction that concurs with experimentally observed trends.

Acknowledgement—This work was performed under Contract N00014-90-J-1556 from the Office of Naval Research to one of the authors (YW). The authors wish to thank the program manager, Dr. Y. Rajapakse, of the Mechanics Division, Engineering Sciences Directorate, for his encouragement and support.

REFERENCES

Aboudi, J. (1991). *Mechanics of Composite Materials*. Elsevier, Amsterdam, The Netherlands.

Budiansky, B. and Fleck, N. A. (1992). Compressive failure of fibre Composites. *J. Mech. Phys. Solids* **41,** 193–211.

Camponeschi, E. T., Jr. (1991). Compression of composite materials: a review. In *Composite Materials: Fatigue and Fracture* (ASTM STP 1110), pp. 550–578. American Society for Testing and Materials, Philadelphia, PA, USA.

Chung, I. and Weitsman, Y. J. (1994a). A mechanics model for the compressive response of fiber reinforced composites. *Int. J. Solids Struct.* **1,** 2519–2536.

Chung, I. and Weitsman, Y. J. (1994b). Model for the micro-buckling/micro-kinking compressive response of fiber-reinforced composites. In Mechanics USA 1994 (Edited by A. S. Kobayashi); *Appl. Mech. Rev.* **47,** Part 2, S256–S261.

Davis, J. G. Jr (1975). Compressive strength of fiber-reinforced composite materials. In *Composite Reliability* (ASTM STP 580) pp. 364–377 American Society for Testing and Materials, Philadelphia, PA, USA.

Davy, P. J. and Guild, F. J. (1988). The distribution of interparticle distance and its application in finite element modeling of composite materials. *Proc. R. Soc.* **A418,** 95–112.

Dixon, W. J. and Massey, F. J. (1969). *Introduction to Statistical Analysis*. McGraw Hill–Kogakusha, New York, NY, USA.

Evans, A. G. and Adler, W. F. (1978). Kinking as a mode of structural degradation in carbon fiber composites. *Acta Metall.* **26,** 725–738.

Garg, S. K., Svalbonas, V. and Gurtman, G. A. (1973). *Analysis of Structural Composite Materials*, Marcel Dekker, New York, NY, USA.

Greszczuk, L. B. (1975). Microbuckling failure of circular fiber-reinforced composites. *AIAA J.* **13,** 1311–1318.

Guynn, E. G., Ochoa, O. O., and Bradley, W. L. (1992). A parametric study of variables that affect fiber microbuckling initiation in composite laminates: Part 1: Analyses. *J. Compos. Mater.* **26,** 1594–1616.

Hahn, H. T. and Williams, J. G. (1986). Compression failure mechanisms in unidirectional composites. In *Composite Materials: Testing and Design* (ASTM STP 893) pp. 115–139. American Society for Testing and Materials, Philadelphia, PA, USA.

Hermann, L. R., Mason, W. E., and Chan, S. T. K. (1967). Response of reinforcing wires to compressive states of stress. *J. Compos. Mater.* **1,** 212–226.

Highsmith, A. L., Davis, J. J. and Helms, K. L. E. (1992). The influence of fiber waviness on the compressive behavior of unidirectional continuous fiber composites. In *Composite Materials: Testing and Design* (*ASTM STP* 1120), pp. 20–36. American Society for Testing and Materials, Philadelphia, PA, USA.

Johnston, N. J., Towell, T. W. and Hergenrother, P. M. (1991). Physical and mechanical properties of high performance thermoplastic polymers and their composites. *Thermoplastic Composite Materials* (Edited by L. A. Carlsson), pp. 27–71. Elsevier Science Publishers, Barking, Essex, UK.

Kyriakides, S. and Liechti, K. M. (1993). Private communication.

Lamborn, M. J. and Schapery, R. A. (1993). An investigation of the existence of a work potential for fiber-reinforced plastic. *J. Compos. Mater.* **27,** 352–382.

Lanir, Y. and Fung, Y. C. B. (1972). Fiber composite columns under compression. *J. Compos. Mater.* **6,** 387–401.

Lin, K. Y. and Zhang, X. J. (1992). Effect of fiber waviness on the compressive strength of laminated composites. In *Proceedings of the 2nd International Symposium on Composite Materials and Structures* (Edited by C. T. Sun and T. T. Loo), Beijing, China, pp. 120–125.

Morley, J. G. (1987). *High Performance Fiber Composites*. Academic Press, New York, NY, USA.

Na, T. Y. (1979). *Computational Methods in Engineering Boundary Value Problems*. Academic Press, New York, NY, USA.

Piggott, M. R. (1993). Compressive strength of composites: how to measure it and how to improve it. In *Advanced Composites '93* (*Proceedings of the International Conference on Advanced Composite Materials* (*ICACM*). Wollongong, Australia, 15–19 February, 1993, (Edited by T. Chandra and A. K. Dhingra), pp. 51–59. TMS Publication.

Piggott, M. R. and Harris, B. (1980). Compression strength of carbon, glass and kevlar-49 fibre reinforced polyester resins. *J. Mater. Sci.*, **15,** 2523–2538.

Rosen, B. W. (1965). Mechanics of composite strengthening. *Fiber Composite Materials*, pp. 37–75, American Society for Metals, Metals Park, Ohio, USA.

Sadowsky, M. A., Pu, S. L. and Hussain, M. A. (1967). Buckling of microfibers. *J. Appl. Mech.* **34,** 1011–1016.
Wang, A. S. D. (1978). A nonlinear microbuckling model predicting the compressive strength of unidirectional composites. *ASME Paper* 78-*WA*/*Aero*-1, 1–8.
Washizu, K. (1975). *Variational Methods in Elasticity and Plasticity*. Pergamon Press, Oxford, UK.
Weitsman, Y. and Chung, I. (1994). Can the compressive response of fiber-reinforced composites be modelled by layered arrays? Report ESM94-1.0-CM, Department of Engineering Science and Mechanics, University of Tennessee.
Yin, W. L. (1992). A new theory of kink band formation. *AIAA*-92-2552-*CP*, 3028–3035.

APPENDIX

Upon putting $\xi_i = \mathrm{d}\psi_i/\mathrm{d}X$, the non-dimensionalized governing equations (18) and (19) read

$$\left.\begin{aligned} &-\lambda^2(Y+Y_0)+\alpha_f^2 Y+\sum_{i=1}^{M} w_i\left(-\alpha_f^2 y_i+\alpha_m^2\frac{\phi_{mi}}{\phi_{fi}}F_i\right)=0\\ &\frac{\mathrm{d}\xi_i}{\mathrm{d}X}+\alpha_f^2(Y-\psi_i)-\alpha_m^2 F_i=0\\ &\frac{\mathrm{d}\psi_i}{\mathrm{d}X}=\xi_i \quad (i=1,\ldots M). \end{aligned}\right\} \tag{A1}$$

The first equation applies to the entire composite, as implied by the summation over all the Voronoi cells, whereas the second and third apply to the M individual cells. We thus have $2M+1$ equations. This system of non-linear coupled differential equations can be converted into algebraic equations by means of a finite differences scheme.

Let N denote the number of nodes along the buckling span, resulting in $N-1$ intervals of length ΔX and mid-nodes. For the mid-node between the nth and $(n+1)$th nodes, which is indicated by $n+1/2$ in the following, the finite difference version of eqn (A1) is

$$-\lambda^2(Y_{n+1/2}+Y_{0,n+1/2})+\alpha_f^2 Y_{n+1/2}+\sum_{i=1}^{M} w_i\left(-\alpha_f^2\psi_{i,n+1/2}+\alpha_m^2\frac{\phi_{mi}}{\phi_{fi}}F_{i,n+1/2}\right)=0$$

$$\frac{\xi_{i,n+1}-\xi_{i,n}}{\Delta X}+\alpha_f^2(Y_{n+1/2}-\psi_{i,n+1/2})-\alpha_m^2 F_{i,n+1/2}=0 \qquad \frac{\psi_{i,n+1}-\psi_{i,n}}{\Delta X}=\xi_{i,n+1/2}. \tag{A2}$$

At this stage, the non-linearity due to a non-linear matrix response expressed by $\mathrm{F}(\gamma_{xy})$ is still retained within the system. This non-linearity can be eliminated by considering the incremented quantities $Y+\delta Y$, $\xi+\delta\xi$, and $\psi+\delta\psi$, which satisfy eqns (A2). Linearization is then achieved upon expanding the non-linear terms in Taylor series, and retaining the first-order terms only. The first of eqns (A2) then results in

$$\delta Y_{n+1/2}=\frac{1}{\sum_{i=1}^{M} w_i Q_{i,n+1/2}-\lambda^2}\left(R_{n+1/2}+\sum_{i=1}^{M} w_i P_{i,n+1/2}\delta\psi_{i,n+1/2}\right) \tag{A3}$$

where

$$P_{i,n+1/2}=\alpha_f^2-\alpha_m^2\left(\frac{\mathrm{dF}}{\mathrm{d}\gamma}\right)_{i,n+1/2}$$

$$Q_{i,n+1/2}=\alpha_f^2+\alpha_m^2\frac{\phi_{fi}}{\phi_{mi}}\left(\frac{\mathrm{dF}}{\mathrm{d}\gamma}\right)_{i,n+1/2}$$

$$R_{n+1/2}=\lambda^2(Y_{n+1/2}+Y_{0,n+1/2})-\alpha_f^2 Y_{n+1/2}+\sum_{i=1}^{M} w_i\left(\alpha_f^2\psi_{i,n+1/2}-\alpha_m^2\frac{\phi_{mi}}{\phi_{fi}}\mathrm{F}_{i,n+1/2}\right).$$

As shown in eqn (A3), δY, which is common to all cells, can be represented explicitly in terms of the other variables $\delta\psi_i$. This enables δY to be substituted into the remaining equations (A2). The substitution of eqn (A3) into the truncated Taylor expansions of the last two of equations (A2) yields the following:

$$\frac{\delta\xi_{i,n+1}-\delta\xi_{i,n}}{\Delta X}+\sum_{k=1}^{M} T_{k,i,n+1/2}(\delta\psi_{k,n+1}+\delta\psi_{k,n})-\frac{Q_{i,n+1/2}}{2}(\delta\psi_{i,n+1}+\delta\psi_{i,n})=U_{i,n+1/2}$$

$$-\left(\frac{\delta\xi_{i,n+1}+\delta\xi_{i,n}}{2}\right)+\frac{\delta\psi_{i,n+1}-\delta\psi_{i,n}}{\Delta X}=V_{i,n+1/2} \tag{A4}$$

where

$$S_{i,n+1/2} = -\frac{\xi_{i,n+1}-\xi_{i,n}}{\Delta X} - \alpha_f^2(Y_{n+1/2}-\psi_{i,n-1/2}) + \alpha_m^2 F_{i,n+1/2}$$

$$T_{k,i,n+1/2} = \frac{w_k P_{k,n+1/2} P_{i,n+1/2}}{2\left(\sum_{i=1}^{M} w_i Q_{i,n+1/2} - \lambda^2\right)}$$

$$U_{i,n+1/2} = S_{i,n+1/2} - \frac{P_{i,n+1/2} R_{n+1/2}}{\left(\sum_{i=1}^{M} w_i Q_{i,n+1/2} - \lambda^2\right)}$$

$$V_{i,n+1/2} = -\frac{\psi_{i,n+1}-\psi_{i,n}}{\Delta X} + \xi_{i,n+1/2}.$$

It should be noted that eqns (A4) apply to each individual cell. Thus we have M values of ξ_i and ψ_i at any mid-node. Collecting $\delta\xi_i$ and $\delta\psi_i$s and forming the vectors

$$\{\delta\xi\} = \{\delta\xi_1, \delta\xi_2, \ldots \delta\xi_M\}^T$$

$$\{\delta\psi\} = \{\delta\psi_1, \delta\psi_2, \ldots \delta\psi_M\}^T$$

eqn (A4) can be expressed in matrix notation as

$$[B_n]\begin{Bmatrix}\{\delta\xi_{n-1}\}\\ \{\delta\psi_n\}\end{Bmatrix} + [A_n]\begin{Bmatrix}\{\delta\xi_n\}\\ \{\delta\psi_{n-1}\}\end{Bmatrix} + [C_n]\begin{Bmatrix}\{\delta\xi_{n+1}\}\\ \{\delta\psi_{n+2}\}\end{Bmatrix} = \{D_n\}. \tag{A5}$$

Here, A_n, B_n, and C_n are $2M$ by $2M$ matrices, and D_n is a $2M$ by 1 vector. Their components are given by

$$B_n(i, M+i) = -\frac{1}{\Delta X}$$

$$B_n(M+i, M+k) = T_{k,i,n+1/2}$$

$$B_n(M+i, M+i) = T_{i,i,n+1/2} - \frac{Q_{i,n+1/2}}{2}$$

$$A_n(i, i) = -\tfrac{1}{2}$$

$$A_n(i, M+i) = \frac{1}{\Delta X}$$

$$A_n(M+i, i) = -\frac{1}{\Delta X}$$

$$A_n(M+i, M+k) = T_{k,i,n+1/2}$$

$$A_n(M+i, M+i) = T_{i,i,n+1/2} - \frac{Q_{i,n+1/2}}{2}$$

$$C_n(i, i) = -\tfrac{1}{2}$$

$$C_n(M+i, i) = \frac{1}{\Delta X}$$

$$D_n(i) = V_{i,n+1/2}$$

$$D_n(M+i) = U_{i,n+1/2}.$$

In the above, the ranges of k and i are $k = 1, \ldots i-1, i+1, \ldots M$, and $i = 1, \ldots M$, respectively.

Denote $\{\{\delta\xi\}\{\delta\psi\}\}^T$ by $\{\Phi\}$. The governing equation for the entire length of the composite is then obtained by collecting eqn (A5). We therefore have

$$\begin{bmatrix}
[A_1] & [C_1] & & & & 0\\
[B_2] & [A_2] & [C_2] & & & \\
 & & \ddots & & & \\
 & & [B_{N-2}] & [A_{N-2}] & [C_{N-2}] & \\
0 & & & [B_{N-1}] & [A_{N-1}] &
\end{bmatrix}
\begin{Bmatrix}\{\Phi_1\}\\ \{\Phi_2\}\\ \vdots\\ \{\Phi_{N-2}\}\\ \{\Phi_{N-1}\}\end{Bmatrix} =
\begin{Bmatrix}\{D_1\}\\ \{D_2\}\\ \vdots\\ \{D_{N-2}\}\\ \{D_{N-1}\}\end{Bmatrix}. \tag{A6}$$

This banded algebraic equation can be readily solved by means of the LU decomposition [Na (1979)]. Since the solution Φ is a vector of increments, it is accumulated at each iterative step to compute ξ and ψ. At the end of each iteration, the norm of Φ is calculated to check for convergence. When it becomes sufficiently small, the iteration is halted, and cumulative values of ξ and ψ are regarded as the convergent solution. The parameter δY is computed by using eqn (A3) and accumulated in the same manner to obtain Y. Deflection, curvature, stress components, and other quantities are computed by means of a post-processing subroutine.

To determine the buckling load, both low and high bounds of applied stress and number of computation intervals are inputed in the program. The highest load value that still gives a convergent solution is taken to be the buckling load.

As shown in Fig. 5, an unloading process is observed in the post-buckling regime. In contrast with the presumed linear elastic behavior of the fibers, it is necessary to define clearly the stiffness of the matrix during unloading. For that purpose, isotropic hardening and elastic unloading of the matrix were assumed. This choice of unloading behavior was guided by data for graphite/epoxy (Lamborn and Schapery, 1993), which approximated to elastic unloading to some extent.

The post-buckling analysis employs the buckling solution as a starting stage, which establishes all the initial values of strains and displacements that correspond to the buckling load, P_{cr}. The post-buckling computation postulates a location X^* in the most recently failed cell, which extends the region of failed matrix in that cell to $X^* < X < 1/2$. Consequently, that region, like previously failed matrix regions under P_{cr}, does not contribute to the shear stiffness of the composite. Subsequently, the composite is subjected to an assumed load level $P < P_{cr}$, and the numerical scheme is employed to obtain values of all corresponding stresses and strains. Note that, wherever the scheme predicts unloading, it is programmed to follow a linear elastic unloading path of the matrix. The value of γ at the foregoing location X^* is then compared with γ_u. If $\gamma(X^*) > \gamma_u$ the level of the load P is reduced iteratively until the establishment of equality, $\gamma(X^*) = \gamma_u$, is within a prescribed tolerance. In this manner, we generate the load–deflection curve in the post-buckling regime.